Properties of metastable states of small dications

Tereza Šedivcová

A thesis presented for the degree of
Doctor of Philosophy

Department of Physical and Macromolecular Chemistry
Faculty of Natural Sciences, Charles University in Prague
Czech Republic
Centre for Biomolecules and Complex Molecular Systems
Institute of Organic Chemistry and Biochemistry
Academy of Sciences of the Czech Republic

December 2006

Dedicated to

All who feel slightly metastable

„Někdo to vyzkoušet musel. Někdo musel slepou uličku lidského poznání ohledat a ohlásit světu: Tudy ne, přátelé!“

Jára da Cimrman

Properties of metastable states of small dications

Tereza Šedivcová

Submitted for the degree of Doctor of Philosophy
December 2006

Abstract

Highly correlated icMRCI wavefunctions are used to calculate the potential energy and spin-orbit coupling functions for several of the lowest electronic states of the CO^{2+} dication. Using these functions, the positions and lifetimes of the corresponding vibronic states are evaluated by means of both stabilisation and complex-scaling methods within the framework of multichannel Schrödinger analysis. Since the predicted lifetimes agree well with the measured values, exactly the same procedure based on the *ab initio* calculations can be used to determine the positions and widths of the isoelectronic system CS^{2+}. The computed lifetimes of several vibronic states of CS^{2+} are in the range $1\text{ps} < \tau \ll 1\mu\text{s}$, therefore these states govern the second step in the sequential pathway $CS_2^{3+} \rightarrow S^+ + CS^{2+} \rightarrow S^+ + C^+ + S^+$ of the overall three-body Coulomb explosion of CS_2^{3+}.

In terms of the foregoing calculations, an attempt to determine both Vis and IR emission and absorption spectra of CO^{2+} is made. Radiative lifetimes found for transition moment matrix elements and Einstein coefficients $A(i \rightarrow f)$ are evaluated using the complex-scaling method. Unfortunately, when emission is concerned, the radiative lifetimes of $A^3\Sigma^+$ and $b^1\Pi$ electronic states in CO^{2+} are longer than the rate of predissociation from these states, which makes it impossible for emission to occur. The absorption spectra of $A^3\Sigma^+ \leftarrow X^3\Pi$ and $b^1\Pi \leftarrow a^1\Sigma^+$ are determined and their absolute intensities are calculated. Also the rotational structure (energy positions and widths) for these transitions is evaluated.

Statement

The work in this thesis is based on research carried out under the supervision of Ing. Vladimír Špirko, DrSc. at the Department of Physical and Macromolecular Chemistry, Faculty of Natural Sciences, Charles University in Prague, Czech Republic. Furthermore, no part of this thesis has been submitted elsewhere for any degree or qualification and it is all my own work unless referenced to the contrary in the text.

Acknowledgments

First of all, I would like to thank Filip for his continuous support and warm smile.

I wish to express my gratitude to Vladimír Špirko for his patient guidance and kind supervision during my postgraduate studies and for fruitful consultations.

Last but not least, thanks to Jiří Fišer and Petra Kaprálová for helping me to understand the theoretical background and all the people close to me for the harmonious social background — namely Luboš Vrbka, Robert Vácha and Babak Minofar. Also thanks to M. Imran for having prepared of this template.

Table of contents

Abstract **iv**

Declaration **v**

Acknowledgments **vi**

Part A. Lifetimes of metastable states of diatomic dications **1**

1 Introduction **2**

2 Theoretical approach **6**
2.1 Complex scaling 7
2.2 The stabilisation method 9

3 Computational details **11**
3.1 Potential energy curves and spin-orbit couplings 11
3.2 Parameters of the methods 11

4 Summary of Results **13**

Part B. Radiative properties of CO^{2+} **17**

5 Introduction **18**

6 Theory **21**
6.1 Coupled potential matrix 21
6.2 Probability of a transition 22
6.3 Intensities 26

7 Calculated spectra **27**
7.1 Emission spectra 27
7.2 Absorption spectra 28

List of Abbreviations **33**

Reference **34**

Appendix **38**

A Complex-scaling method **38**

A.1 The basic idea 38

A.2 Several approaches to avoid fitting *ab initio* potential 38

A.2.1 Scaling of basis functions 38

A.2.2 Complex absorbing potential (CAP) 39

A.2.3 Smooth-exterior-complex-scaling (SECS) 39

B Intensity line profile **41**

List of Publication **43**

Selected reptints and preprints **44**

Part A. Lifetimes of metastable states of diatomic dications

Chapter 1

Introduction

The first mention of dication was in 1931 [1]. The dissociation products formed by bombarding nitrogen and carbon monoxide with electrons of a definite velocity were studied with a mass spectrograph. Due to the fast development of measuring techniques and methodology over the last decade, the multiply-charged molecular ions and their interactions with electrons and neutral atoms/molecules are no longer regarded as curiosities. These species and the reactions in which they are involved are of importance not only in hot astrophysical and terrestrial plasma but also in low-temperature systems. Excellent reviews describing both experimental and theoretical approaches for studying multiply-charged ions are in Ref. [2, 3]. Information about some branches where dications are worth studying is outlined below.

Small dications were first identified in nature in the upper atmosphere of the Earth, where terrestrial plasma is formed by hard radiation. Gases in this environment can be inner-shell ionised (i) by the absorption of X-ray solar radiation, (ii) by collision with energetic protons or electrons, and (iii) on impact with high-velocity oxygen or hydrogen atoms. Both model calculations on the one hand and rocket and satellite experiments on the other show that the Auger effect on excitation and ionisation processes is the main source of energetic electrons with an energy between 315 and 510 eV, an essential source of doubly-charged positive ions in the upper atmosphere, and the main source of the electronic excitation of these ions [4]. In this respect, metal ablation from meteorites and abandoned spacecrafts is particularly relevant because of the low ionisation energies of metals. The same processes also occur in the atmosphere in the case of other objects. For instance, N_2^{2+} is expected to be detected on Titan by the CASSINI project [5] and CO^{2+} in the daytime ionosphere of Mars [6].

Another main area where dications have been proved is the Interstellar Medium (ISM). They are Fullerenes [7] and Polycyclic Aromatic Hydrocarbons (PAHs) [8]. Both these from our point of view extensive systems (50–200 carbon atoms) seem to be responsible for the unidentified IR bands which have been observed in a number of astrophysical sources. PAHs dominate the heating and cooling of ISM via photoelectric ejection [9]. Malloci *et al.* [8] have shown that the PAH dications ($PAHs^{2+}$) are

as important for the understanding of ISM as PAH neutrals or cations. A systematic theoretical study on 40 $PAHs^{2+}$ containing up to 66 carbon atoms has confirmed that PAHs could reach the doubly-ionised state in HI regions. The total integrated IR absorption cross-sections indicate a marked increase upon ionisation, on average approximately two and five times greater for $PAHs^{2+}$ than for $PAHs^{+}$ and PAHs, respectively. The visible-UV photo-absorption cross-sections for the 0, +1 and +2 charge-states exhibit comparable features, but between 7 and 12 eV $PAHs^{2+}$ are found to absorb slightly less than their parent neutrals and singly ionised species [8]. Having combined these pieces of information, it was discovered that $PAHs^{2+}$ should actually be more resilient to photodissociation than PAHs and $PAHs^{+}$, provided that dissociation thresholds remain nearly unchanged by ionisation.

The role of dications has been underestimated also in simple reactions. The idea still prevails, particularly when considering electron-molecule collisions, that the cross-section for molecular double ionisation forms only one or two percent of the single ionisation cross section, even at significant ionising energies (> 50 eV). As a result, the consequences of multiple ionisation were considered unimportant when identifying ion-molecule reactions and studying the generated data for models of ionised media. However, recent experiments have shown that in many cases molecular double ionisation cross sections have been significantly underestimated, due to experimental deficiencies in detecting the energetic fragments from dissociative double ionisation [10]. When such fragments are efficiently collected, it is clear that in electron-molecule collisions, even at electron energies close to threshold, double ionisation can significantly contribute to the ion yield. In addition, experimental and theoretical investigations have shown that many molecular dications can, in certain electronic states, live for extended periods [11]. It has thus become clear that the consequences of molecular double ionisation and the bimolecular chemistry of molecular dications are worth investigating.

The bimolecular reactions containing dications are atypical as they usually generate a pair of monocationic products which possess, due to their mutual repulsion, significant kinetic energies. A typical value of possessed kinetic energy is at least 6 eV for an ion pair formed from a diatomic dication. Such energy releases are equivalent to a reaction exothermicity of approximately 600 kJ/mol, a value comparable with many of the chemical reactions used to propel rockets. Products with such high translational energies are not generated by conventional monocation-neutral reactions and may exert some influence on the chemistry of energised media.

Dications are important not only as potential ion engines but also as antimicrobial agents. Dicationic compounds based on pentamidine have shown impressive antimicrobial activity against a variety of organisms [12, 13]. Dicationic molecules with improved efficacy and reduced toxicity comparable to pentamidine have been reported in animal models of *pneumocystosis* [14] and *cryptosporidiosis* [15]. Many such compounds also demonstrate excellent activity against *Leishmania* parasites. The antileishmanial activity of several such dicationic molecules was mentioned in

1990 [16]. J. Brendle *et al.* reported [13] the in vitro evaluation of 58 aromatic cations against axenic amastigote-like *Leishmania donovani*. In that assay, some of the dicationic agents proved to be more potent than pentamidine, thus indicating that the synthesis of new aromatic dications could lead to the development of more effective antileishmanial agents.

In fact, many dications derived from small stable molecules are thermodynamically unstable, with the dication having an energy greater than that of the relevant pair of separated singly-charged fragments [17, 18]. However, chemical bonding can quite often overcome this repulsion and make these ions rather stable or, at least, metastable in the long term. A key stability aspect concerns the relative positions of the potential energy asymptotes of the ions and the corresponding charge-separated fragments, as well as the positions of the molecular vibronic levels. The stability of the individual molecular states also depends strongly on the shape of the potential energy curves, their relative positions and interstate couplings. Consequently, the actual lifetimes achieve values which may vary over a quite wide range.

For instance, the lifetime of the $v = 0$ vibrational level of the volcanic $^1\Sigma_g^+$ state of He_2^{2+}, which autodissociates into $He^+ + He^+$ fragments, has been calculated to be extremely long, namely 220 min [19]. This finding, together with the high energy content of He_2^{2+} and its small mass, offers the possibility of new physical and chemical reactions for the release of propulsive energies in the range of 230–1000 kcal/mol, with specific impulses much higher than those of the existing liquid hydrogen and oxygen fuels. Also the other molecular dications in which rare-gas atoms are one type of the constituents are often known to possess bonds that are surprisingly strong, despite the chemical inertness of rare-gas atoms. High-level quantum-chemical studies have predicted that several such species may be thermodynamically stable against unimolecular dissociation [20]. Many such dication species have been generated using a variety of techniques. Species like $XeNe^{2+}$, $XeAr^{2+}$ and $KrNe^{2+}$ have been generated by low-energy electron bombardment of the respective neutral van der Waals dimers formed using supersonic expansion techniques [21]. Determining the lifetimes of the dications formed from CO, CO_2, SO_2 and other species which cause the greenhouse effect is crucial to ascertaining how to reduce the massive amount of greenhouse gases in our atmosphere.

In this part of the study, we would like to be helpful in establishing which of the channels of CS_2^{3+} fragmentation:

(a) $CS_2^{3+} \rightarrow S^+ + CS^{2+} \rightarrow S^+ + C^+ + S^+$

or (1.1)

(b) $CS_2^{3+} \rightarrow S^+ + C^+ + S^+$

is more reliable. The creation of molecular ions in charge states greater than 2 is almost always followed by a charge separation reaction. A triply charged polyatomic molecule, M^{3+}, can dissociate into a number of possible channels (e.g., $M^{3+} \rightarrow A^{2+} + B^+ + C$, $M^{3+} \rightarrow A^+ + B^+ + C^+$, $M^{3+} \rightarrow AB^+ + C^{2+}$, etc.). Complete charge separation appears to be the most likely. However, the channel resulting in

the formation of one or more neutral products accompanying charge separation has been shown to be the main process in charge-separation studies of such species as triply charged benzene ions [22]. Analogous dissociation can occur either through simultaneous Coulomb explosions or a sequential process in which an intermediate charged fragment dissociates in a subsequent reaction. The CS_2^{3+} fragmentation reaction has recently been studied [23] as three-body Coulomb explosion decays of CS_2. It arises from this experiment that if the process (a) in reaction (1.1) had more probability, some of the quasibound vibronic states of CS^{2+} would have lifetimes ranging from 10 ps to 1 μs. Since there is a lack of experimental data about CS^{2+}, we rely on the much more studied isoelectronic system, the CO^{2+} dication, to verify the accuracy of both the employed *ab initio* calculations and methods for the determination of the lifetimes of metastable states.

Despite the fact that CO^{2+} is one the most studied dications, the theoretical works offer only rough data concerning lifetimes that would differ from the experiment [24, 25]. These discrepancies have their origin mainly in the inclusion of only one electronic state into calculations of widths of vibronic states, thus not taking into account e.g. the spin-orbit interaction. This interaction takes place mainly if the ground state close to the minimum of the potential well is crossed by a repulsive state. Another problem can be caused by applying improper methods or merely improperly converged parameters. Unlike the energies of vibronic states, their widths are very sensitive not only to the correctness of potential curves and electronic coupling functions but also to the parameters used (θ, the box size, the number of bases, etc., described in the following chapters).

The authors of the CS_2 Coulomb explosion made a mistake when calculating the lifetimes of CS^{2+}. By assuming that CS^{2+} is mostly prepared in the $X^3\Pi$ state and trapped in the bound part of the potential, τ was estimated using the theoretical potential energy curve of the $X^3\Pi$ state, $V(r)$, by the semiclassical WKB method [26]. This idea lead to the conclusion that the lifetimes of CS^{2+} are too long for the sequential pathway (a) of the fragmentation CS_2^{3+} reaction (1.1). Nevertheless, the set of the observed momentum vectors of the fragment ions determined for their respective explosion events exhibits a clear trajectory, originating from the rotational motion of an intermediate CS^{2+} ion, formed in a sequential explosion process of CS_2^{3+} prior to the complete three-body fragmentation.

In the first step, the predissociation rates in the CO^{2+} dication are calculated using an accurate theoretical procedure involving the ground state and 5 excited electronic states. The required potential energies and the spin-orbit coupling functions are evaluated using internally contracted multi-reference configuration interaction (icMRCI) wavefunctions. The numerically "exact" (multichannel) predissociation rates/lifetimes, accounting for the spin-orbit interactions, are determined using the stabilisation [27–29] and complex-scaling methods [30, 31]. Consequently, the same procedures are applied when evaluating lifetimes of the vibronic state of CS^{2+}.

Chapter 2

Theoretical approach

A precise definition of resonance or the metastable state has been a matter of a great deal of debate in the literature (see [32] and references therein). As the notion of resonance lacks sufficient clarity, different criteria are used for identifying resonances and determining their parameters. From a quantum mechanic point of view, resonance is a quantum state whose mean energy lies above the fragmentation threshold of a system and is associated with:

(a) a pronounced variation of the cross sections if the fragmentation energy lies in the vicinity of the energy of the resonance (energy-dependent definition) — the width of this neighbourhood is called the width of the resonance.

(b) an exponential decay of the system when the system has a mean energy close to the resonance energy (time-dependent definition) — the lifetime of the resonance is proportional to the inverse of its width. Resonances are usually classified into shape and Feshbach resonances or into Breit-Wigner and Fano resonances.

In quantum field theory, resonance is an unstable particle or a state. It is characterised by a complex pole off the real line in the S-matrix (which happens to be analytic). A sharp resonance is a resonance with a sharp peak in the S-matrix (which corresponds to a long lifetime compared to the reciprocal of its mass) while a broad resonance is a resonance with a spread-out peak (which corresponds to a short lifetime relative to the reciprocal of its mass). If a resonance is too broad, it might not be considered as a state at all even if it has a complex pole (far from the real line).

It arises from these definitions that lifetimes of a metastable state should be calculated using complex analysis and quantum field theory. Fortunately, several approximations have been developed, two of which, the complex-scaling and stabilisation method, have been used in this study. These two approaches can work with multidimensional and multichannel problems, which makes it possible for the spin-orbit (s-o) interaction to be taken into account. The main points used in the presented calculations are briefly described below. Further details are in Ref. [11,33] and references therein and in the Appendix A.

2.1 Complex scaling

In the complex-scaling (c-s) method [30], the sought resonance characteristics are obtained from complex eigenvalues of a c-s Hamiltonian. The advantage of this method is that the eigenfunctions associated with complex resonance eigenvalues are square-integrable, thus the Schrödinger equation can be solved by bound-state techniques. The c-s Hamiltonian $\hat{H}_\theta(R)$ is obtained from the physical Hamiltonian $\hat{H}(R)$ by complex scaling of the coordinate R, such that $\hat{H}_\theta(R) = \hat{H}(Re^{i\theta})$, where θ is a c-s parameter $0 \leq \theta < \pi/4$. The c-s Hamiltonian for diatomic dissociation is obtained by complex transformations of the kinetic energy operator, potential, and s-o coupling, such that

$$\hat{H}_\theta(R) = -e^{-2i\theta}\frac{\hbar^2}{2\mu}\frac{d^2}{dR^2} + \hat{V}(Re^{i\theta}), \tag{2.1}$$

with the approach being that the potentials are coupled with each other by the s-o operator $\hat{H}_{SO}$. The complex transformation of s-o coupling is straightforward also as $\hat{H}_{SO\theta}(R) = \hat{H}_{SO}(Re^{i\theta})$. Resonances are obtained as solutions of $\hat{H}_\theta(R)$ and are characterised by θ-independent complex eigenvalues. The complex resonance eigenvalues,

$$\epsilon = E_{\text{res}} - \frac{i}{2}\Gamma_{\text{res}}, \tag{2.2}$$

define the resonance positions E_{res} and widths Γ_{res}, respectively. Resonance states appear in the spectrum of $\hat{H}_\theta(R)$ for θ larger than the critical value given by

$$\theta_c = \frac{1}{2}\arctan\frac{\Gamma_{\text{res}}}{2E_{\text{res}}}. \tag{2.3}$$

The eigenfunctions and eigenvalues of $\hat{H}_\theta(R)$ are obtained in a finite box using a Fourier basis set as the stationary points with respect to the variation of the scaling parameter [30],

$$\left.\frac{\partial E_{\text{res}}}{\partial\theta}\right|_{\theta_{\text{stat}}} = \left.\frac{\partial\Gamma_{\text{res}}}{\partial\theta}\right|_{\theta_{\text{stat}}} = 0. \tag{2.4}$$

An example of the energy spectrum of the complex-scaled Hamiltonian and a typical θ-trajectory are displayed in the Figs. 2.1 and 2.2, respectively. The energy spectrum corresponds to the five lowest electronic states of the CS^{2+} dication. One can clearly distinguish between five strings of eigenvalues corresponding to the rotated continuum at $\theta = 0.04$ rad.

In order to enable the construction of the c-s Hamiltonian (Eq. 2.1), the molecular Born-Oppenheimer potential energy curves (surface) and coupling functions must be represented by analytical functions, which allows for their analytical continuation to the complex plane $R \rightarrow Re^{i\theta}$. For small values of the θ parameter (up to 0.06 rad), the complicated polynomial expression can be used. The function for fitting used in this study is shown in the following chapter Eq. 3.1 and 3.2, and in Ref. [34]. However, the wider the resonance widths are, the higher θ must be

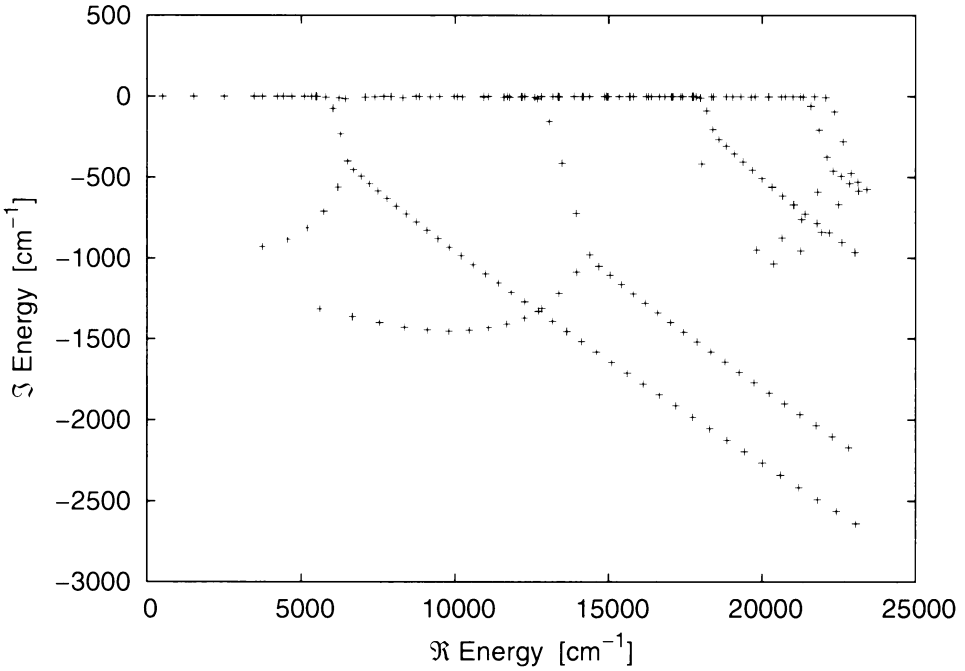

Figure 2.1: The energy spectrum of the complex-scaled Hamiltonian for the five lowest electronic states of CS^{2+} for $\theta = 0.04\,\mathrm{rad}$.

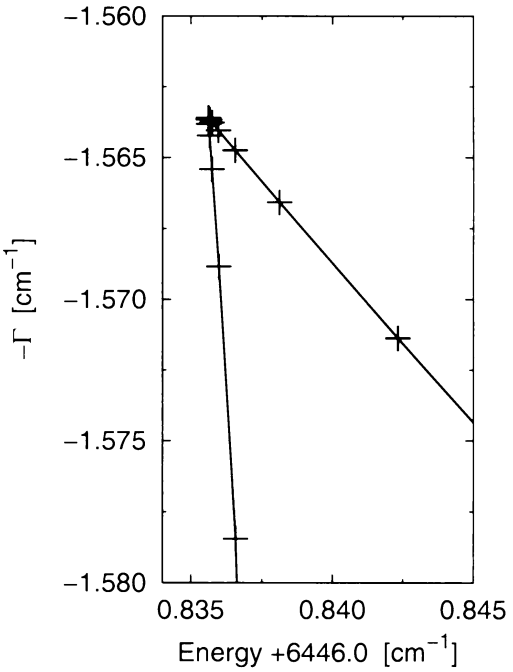

Figure 2.2: The θ-trajectory for the resonance of CS^{2+} localised at $6446.8\,\mathrm{cm}^{-1}$ with θ changed from 0.0001 to 0.06 rad. The stationary point is localised at [6446.837; −1.563].

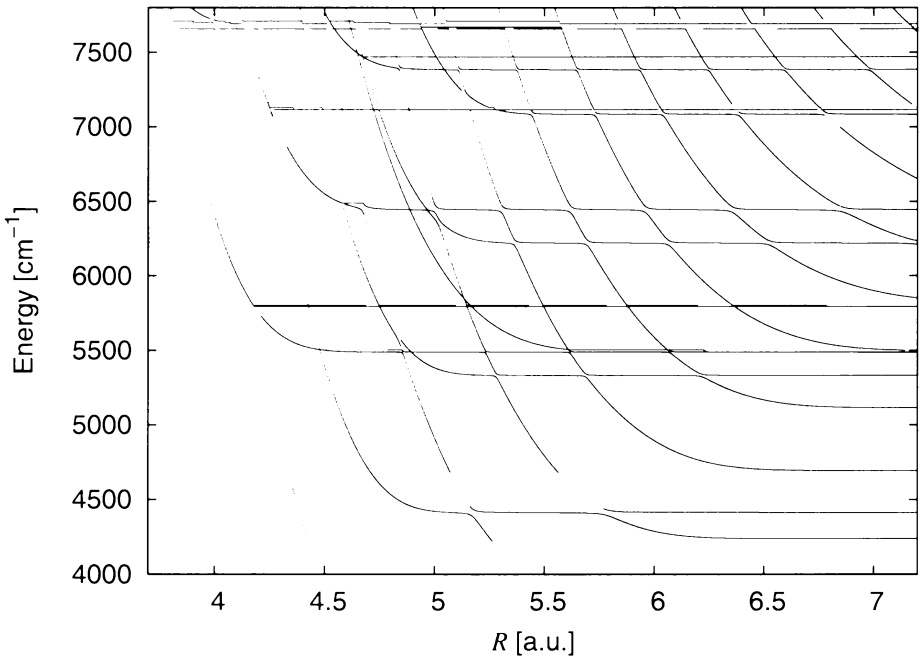

Figure 2.3: Stabilisation diagram: energy eigenvalues E_n vs. the box size (internuclear distances) R of the CS^{2+} dication.

used (e.g., Feshbach resonance in CH^+ [35]). In that case, only simple function representation (fit) of potentials can be applied (e.g., $V(R) = 7.5R^2e^{-R}$). Nowadays, different approaches to complex-scaling are being developed to avoid this [30,36–39]. The main ideas of some are outlined in Appendix A.

2.2 The stabilisation method

The key idea of the stabilisation theory [27–29] is that resonances are localised near the potential well. Putting the whole system in a box of the size L, much larger than the range of this well, results in a new system, which should cover all the localised states but does not have an infinitely dense continuum. Once the finite basis is converged and the range L of this basis becomes much larger than the well region, nothing dramatic should happen to the resonant states while L further increases, whereas all the other states (i.e. the representation of the continuum) must change with L.

To study resonance parameters with the modified stabilisation theory, one needs the set of energy eigenvalues versus the box size L. This implies a repeated diagonalisation of an appropriate Hamiltonian $\hat{H}$ in a series of enclosing boxes with their varying box size L: $L_0 \leq L \leq L_0 + \Delta L$. Plots of the eigenfunction of the Hamiltonian $E(L)$ as a function of L are known as the stabilisation diagram. One example of this diagram is shown in Fig. 2.3. In this case, the box size L is presented as internuclear distance, usually denoted as R expressed in atomic units.

When box normalisation is used, the density of the states is obtained through counting the number of states with energies between E and $E + dE$:

$$\langle \rho(E) \rangle = \frac{-1}{\Delta R} \sum_n (dE_n(R)/dR)^{-1}|_{E_n=E}. \tag{2.1}$$

The local maxima in the density of the states are associated with the resonances. The resonance energy E_{res} and the width Γ_{res} can then be determined by the following Lorentzian fitting:

$$\langle \rho(E) \rangle = \rho_a + \frac{\rho_b(\Gamma_{res}/2)}{(E - E_{res})^2 + \Gamma_{res}^2/4}, \tag{2.2}$$

where ρ_a is a weakly energy-dependent background and ρ_b is a constant to be fitted. The widths of Lorentzian peaks Γ_n are the inverse lifetimes of the resonance states.

Chapter 3

Computational details

3.1 Potential energy curves and spin-orbit couplings

All *ab initio* calculations were carried out using the MOLPRO suite of *ab initio* programs [40]. The atomic orbital basis sets were cc-pV6Z [41]. The molecular orbitals for the configuration interaction (CI) treatment of both the CO^{2+} and CS^{2+} dications were obtained in both the one-state and the state-averaged complete-active-space self-consistent field (CASSCF) calculations with equal weights for the participating states of the same spin multiplicity in the C_{2v} symmetry. The full active space consisted of 1σ 6σ, 1π and 2π orbitals with all electrons (AE) correlated for CO^{2+} and 5σ 8σ, 2π and 3π orbitals for CS^{2+}. The potential energy functions (PEFs) were calculated using the internally contracted multireference configuration interaction (icMRCI) method [42, 43].

The *s-o* integrals were evaluated with the icMRCI wavefunctions, using the Breit-Pauli operator, as implemented in MOLPRO code. Due to the limitation of this program, only the *spdf* orbital subset of the cc-pV5Z basis set with the valence electrons correlated was employed in the *s-o* calculations.

3.2 Parameters of the methods

It should be noted that both the stabilisation and complex-scaling methods can provide accurate estimates only for lifetimes shorter than $10\,\mu$s. In order to obtain fully converged results, the six lowest electronic states: $X^3\Pi$, $a^1\Sigma^+$, $^3\Sigma^-$, $b^1\Pi$, $c^1\Delta$ and $A^3\Sigma^+$ for CO^{2+} and the five lowest ones: $X^3\Pi$, $a^1\Pi$, $^3\Sigma^-$, $b^1\Sigma^+$ and $c^1\Delta$ for CS^{2+} connected by spin-orbit interaction had to be involved in both methods.

The *c-s* calculations were performed using polynomially smoothed adiabatic po-

tential energy ($V(R)$) and s-o coupling ($H_{SO}(R)$) functions

$$V(R) = \frac{\left(\sum_{i=0}^{M} V_i(R+c)^i\right)^2}{\sum_{i=0}^{P} w_i(R+c)^i} e^{-\alpha s(R+c)} + \frac{\sum_{i=0}^{L} a_i(R+c)^i}{\sum_{i=0}^{N} b_i(R+c)^i} + \sum_{i=0}^{K} d_i(R+c)^i \tag{3.1}$$

and

$$H_{SO}(R) = \left(\sum_{i=0}^{M} V_i R^i\right)^s e^{-\alpha R} + \frac{\sum_{i=0}^{L} a_i R^i}{\sum_{i=0}^{N} b_i R^i} + \sum_{i=0}^{K} d_i R^i \tag{3.2}$$

until the highest order of 5 and, naturally, not all elements were used for all potentials. The standard deviation of fits was $\pm 10\,\mathrm{cm}^{-1}$ and $\pm 0.3\,\mathrm{cm}^{-1}$ for all potential and s-o coupling functions, respectively. The Hamiltonian matrices were calculated using discrete variable representation [31]. The actual calculations were achieved variationally using 300 particle-in-box basis functions in the range $1.7 \leq R \leq 7.2$ a.u. for CO^{2+} and $2.2 \leq R \leq 10.2$ a.u. for CS^{2+}, with θ varying from 0.0001 to 0.06 rad with a 0.001 increment.

The actual stabilisation calculations were performed by solving the system of the coupled channel Schrödinger equations

$$\frac{d^2\mathbf{y}(R)}{dR^2} = [\mathbf{V}(R) - E\mathbf{I}]\mathbf{y}(R), \tag{3.3}$$

where the diagonal and off-diagonal elements of the potential energy matrix $\mathbf{V}(R)$ consisted of adiabatic potential energy functions and s-o interactions, respectively; $\mathbf{y}(R)$ was a column vector and $\mathbf{I}$ was the unity matrix. L_0 was fixed at 1.7 a.u. whereas L varied from 1.7 to 6.1 a.u. for CO^{2+} and from 2.2 to 9.9 a.u. for CS^{2+}, by an increment of 0.001 a.u. The equation (3.3) was solved using the renormalised Numerov method [44].

Chapter 4

Summary of Results

Successful calculations of the lifetimes of the vibronic states within the CO^{2+} dication are widely discussed in Ref. [11], which is enclosed as Paper 1. There are shown smooth potential energy curves of nine electronic states and the *s-o* coupling between them (Figs. 1 and 2). These functions were employed for calculating the positions and widths of the experimentally studied vibronic levels (i.e. $v = 0\ 5$ $X^3\Pi$, $v = 0\ 3$ $a^1\Sigma^+$ and $v = 0\ 2$ $b^1\Pi$). It can be seen that for the majority of states, the vibrational energies and widths obtained by both theoretical methods and their parameters described in the preceding chapters differ only very slightly and lie between the respective experimental data. The results from the stabilisation method are even in semi-quantitative agreement. The calculated lifetimes confirm that the spin-orbit induced predissociation is a dominant decay mechanism for CO^{2+}.

Due to very good results for the CO^{2+} dication, the same procedures can also be used to determine the lifetimes of the resonance states of CS^{2+}. The adiabatic PEFs of the ten lowest electronic states of CS^{2+} and the pertinent *s-o* couplings between the five lowest states are shown in Figs. 1 and 2 in Ref. [33], respectively. This work is also enclosed as Paper 2.

The resonance energies, widths (in cm^{-1}) and lifetimes (in μs) determined from the actual calculations are summarised in Table 4.1. Both the stabilisation and complex-scaling methods yield very similar results. These vibronic states are sequenced according to increasing energy regardless of the electronic state, one reason being that there is no straightforward classification. In Ref. [33], we calculate vibronic properties also in the frame of one-dimensional (1D) approach. The results in the 1D calculation are only crude approximants of their genuine values and, with the exception of strongly metastable states, they become highly inaccurate. This is reflected especially in the case of the energy widths, which reach reliable values only for the lowest adiabatic state. In other words, the *s-o* interaction causes heavy mixing of the adiabatic molecular states. After all, only energies and widths are possible to read from experimental spectra.

As far as the three-body Coulomb explosion of CS_2 is concerned, there are several vibronic states meeting the requirement that the lifetimes should be in $1\,\mathrm{ps} < \tau \ll$

Table 4.1: Energy positions (cm^{-1}), widths (cm^{-1}) and lifetimes $\tau(\mu s)$ of the lowest vibronic resonances of CS^{2+} calculated using the stabilisation and complex-scaling approach, with ϵ denoting the widths narrower than $10^{-7}\,cm^{-1}$.

Stabilisation method			Complex scaling		
$E(cm^{-1})$	$\Gamma(cm^{-1})$	$\tau(\mu s)$	$E(cm^{-1})$	$\Gamma(cm^{-1})$	$\tau(\mu s)$
509.87	ϵ		510.42	ϵ	
1521.43	ϵ		1520.80	ϵ	
2509.19	ϵ		2508.45	ϵ	
3473.57	ϵ		3472.62	ϵ	
3754.82	ϵ		3752.94	ϵ	
4239.61	ϵ		4235.76	ϵ	
4414.81	ϵ		4413.56	ϵ	
4695.77	ϵ		4692.79	ϵ	
5114.90	6.9×10^{-6}	0.77	5113.48	3.1×10^{-6}	1.73
5331.68	4.7×10^{-5}	0.11	5330.73	1.0×10^{-6}	5.33
5486.01	5.2×10^{-3}	1.0×10^{-3}	5487.02	2.3×10^{-3}	2.2×10^{-3}
5488.54	3.4×10^{-1}	1.6×10^{-5}	5489.41	1.5×10^{-1}	3.5×10^{-5}
5494.92	1.2×10^{-2}	4.5×10^{-4}	5495.46	6.8×10^{-3}	0.7×10^{-3}
5808.37	8.55	6.2×10^{-7}	5806.63	4.40	1.2×10^{-6}
6221.62	1.93	2.8×10^{-6}	6220.59	0.98	5.3×10^{-6}
6445.75	2.87	1.9×10^{-6}	6446.83	1.56	3.3×10^{-6}
7084.65	1.10	4.8×10^{-6}	7083.66	0.54	9.7×10^{-6}
7383.37	0.56	9.5×10^{-6}	7385.53	0.31	1.7×10^{-5}
7683.74	3.36×10^{-2}	1.5×10^{-4}	7686.78	1.8×10^{-2}	2.9×10^{-4}

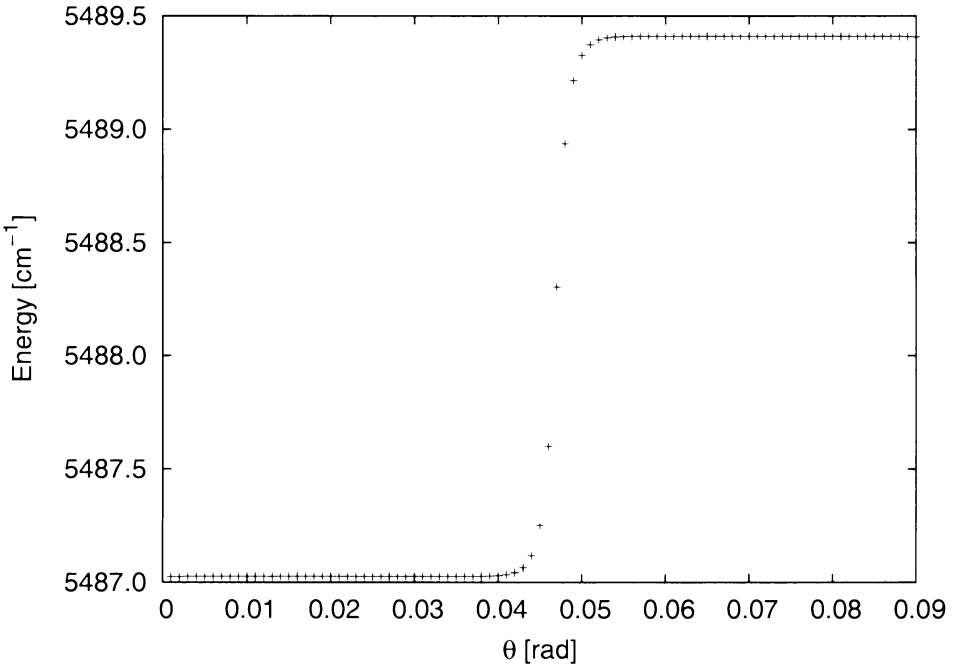

Figure 4.1: The real part of the θ-trajectory (energy position) in dependence on θ. The two different resonances occur for different θ.

$1\,\mu$s as arises from the experiment, such that the sequential reaction is allowed through at least seven vibronic states (see Table 4.1). These results differ from the conclusion drawn by Hishikawa *et al.* [23]. By assuming that CS^{2+} is mostly prepared in the $X^3\Pi$ state and using the WKB estimate for the lifetime of CS^{2+} in this state, they arrived at the conclusion that the *ab initio* potential [45] needs to be lowered, rather unreasonably, by $\sim$1.0 eV to account for the observation. According to our results, the lowest $X^3\Pi$ state is heavily mixed with the firstly excited $^3\Sigma^-$ state, which possesses a much lower dissociation asymptote (see Fig. 3 in Ref. [33]).

We now turn our attention to the case of two very energetically close resonances that are localised at the 5486 and 5488 cm^{-1} energy position. At least one of the resonances seems to be somehow additional as compared with the 1D approximation (see Table III in Ref. [33]). While Table III shows only values from calculations using the stabilisation method, the same resonances also appear during calculations using the *c-s* method. It happened during *c-s* calculations that the 5488 resonance, with a wider width (and thus also a shorter lifetime) than the 5486 resonance, appeared at higher values of θ despite the fact that, based on the relation (2.3), it was expected to be detected already in the $\theta_c \sim 10^{-1}$ rad. The dependence of the energy of resonance states on θ for this area of energy is shown in Fig. 4.1. The same part of energies determined by the stabilisation method is shown in Fig. 4.2. It should be mentioned that the two resonances did not appear in the calculations of either method simultaneously. When one resonance was localised, the other was impossible to determine. Since both resonances appear in calculations of both methods, such

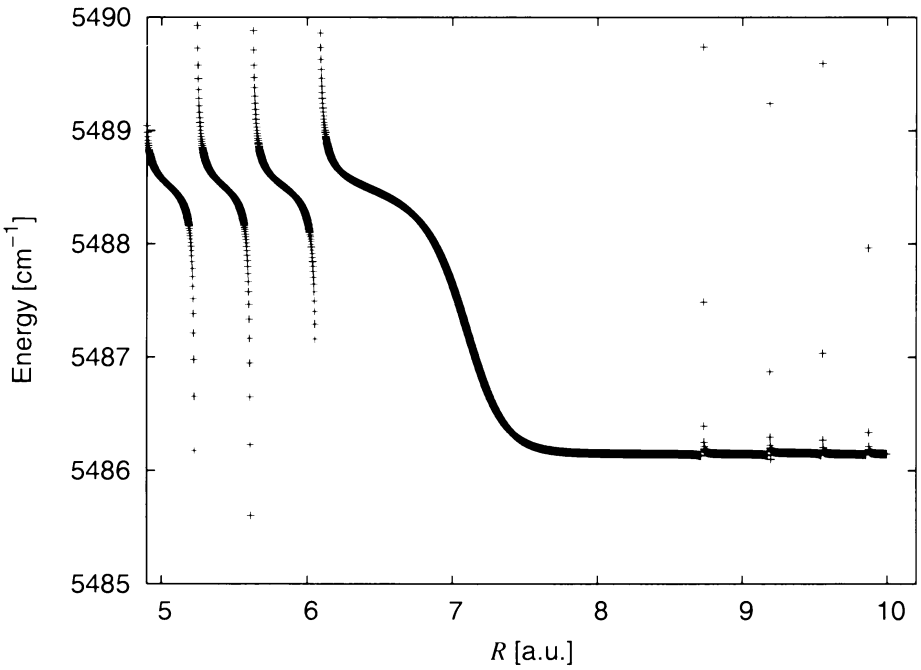

Figure 4.2: The part of the stabilisation diagram around the energy of 5486 cm^{-1}: the two different resonances localised at the energy of 5486 and 5488 cm^{-1}. When one resonance appears, the other vanishes.

a resonance is not an artefact of only one of them. These states are formed due to the s-o interstate interaction and should be measured.

Part B. Radiative properties of CO^{2+} (visible and infrared spectra)

Chapter 5

Introduction

This part of the study focuses on the CO^{2+} dication. It builds on the preceding part using the calculated lifetimes and vibronic resonance wavefunctions from the complex-scaling method and proceeds in the calculation of transition moment functions for several electronic states and transitions using the *ab initio* method and in determining the radiative transition probabilities. The aim is to simulate the rovibronic spectra of CO^{2+} based on the first principles that are believed to be useful in searching for spectral evidence of the CO^{2+} dication both in the laboratory and the interstellar medium.

The first dication to be measured with rotational resolution was N_2^{2+} in 1958 [46], the second was NO^{2+} in 1987 [47], followed by only a few others. These are not many and even nowadays, the spectra of molecular dications with better than vibrational resolution are difficult to obtain and analyse. There is a lack of theoretical prediction of Vis or IR spectra of these species, which makes their identification in spectra almost impossible.

In the astrochemical branch of spectroscopy, only the N_2^{2+} dication has been discussed in the frame of possible detection of this ion layer by a spectrophotometer, and it has been shown that the UVIS instrument on board CASSINI is capable of observing it [5]. The second molecular dication, CO^{2+}, is likely to be present in detectable quantities in some region of the interstellar medium. It is therefore of great interest to determine as many of its spectroscopic and structural properties as possible to be able to conduct future high resolution laboratory and astronomical measurements.

Both emission and absorption spectra and their intensities are required. The emission vibronic spectra of the CO^{2+} dication are questionable, because it is not clear from previous experimental research [48–50] whether emission spectra can be created from the states $A^3\Sigma^+$ and $b^1\Pi$, which is caused by competition between the radiative and predissociation lifetimes. The question of this dication being formed by radiative association is closely connected with this effect. However, it is known that the rotation influences the shape of the potential curves, and the lifetimes depend profoundly on these shapes and their relative positions. Consequently, it

will be quite useful to determine the dependence of the lifetimes on the quantum number J at least for the lowest vibronic levels of the $A^3\Sigma^+$ and $b^1\Pi$ electronic states.

As far as absorption spectra are concerned, the lifetimes of several lowest vibronic states discussed in previous chapters are long enough for catching a photon during an experiment. Nevertheless, the photon having been absorbed, the system dissociates through a barrier due to the *s-o* interaction. As a result, the widths of the absorption spectra are, based on the finite lifetimes of the final state, related to the photodissociation cross-sections.

To identify anything either in astronomical or laboratory spectra is still a challenge. Great attention must be paid here to shift, intensity and line shape. The observed spectral lines are always broadened, partly due to the finite resolution of the spectrometer and partly owing to intrinsic physical causes. Anticipating the natural broadening, the principal physical causes of the spectral-line broadening are Doppler effect and pressure. The numerous factors affecting line shape are described in Appendix. These factors can be combined together and thus provide information about temperature, turbulence, rotation speed, density and/or magnetic field. However, for the prediction of these conditions it is necessary to have a good theoretical model of the natural width of the lines.

One of the aims of this study is to show the correct calculation of the natural width of the spectral peaks behind the Franck-Condon (FC) approximation for CO^{2+}. In our previous studies (Refs. [51] and [52]) we tried to identify C_2^- in the interstellar medium (ISM) and stellar envelope, respectively. As the first step, we looked for, at least, rovibronic-energy positions of the $B^2\Sigma_u^+ \leftarrow X^2\Sigma_g^+$ transition of C_2^- in the ISM spectra. As several correspondences were detected, the FC approximation was applied to determine the intensities. This search for C_2^- was carried out on already measured spectra, hence the relative intensity of the $v = 0\ 0$ band could be used and fitted to a peak in the spectra. Assuming that the Doppler shift and broadening had been eliminated through calibration, the intensity depended only on temperature. The temperature of the ISM in the examined region was approximately $T = 30\,\mathrm{K}$. Unfortunately, there was no success [52].

Nonetheless, it seemed that several lines in the carbon-star envelope HD 56126 spectrum could be compared with the laboratory lines of C_2^-. Accordingly, we tried to calculate the intensities more accurately, including the transition-moment functions [51] (enclosed as Paper 4). The potential energy curves of the $^2\Sigma_g^+$, $^2\Pi$ and $^2\Sigma_u^+$ states of C_2^- were constructed by morphing highly accurate icMRCI *ab initio* potentials. The resulting potentials reproduced all of the observed rovibronic data, enabling thus the evaluation of the highly reliable rovibronic wavefunctions of all the observed molecular states. Electronic transition moment functions for the dipole made it possible for transitions among the studied states to be evaluated from a highly correlated icMRCI wavefunction. Using these functions and the rovibronic wavefunctions pertaining to the morphed potential energy curves, reliable dipole mo-

ment matrix elements were evaluated for all the studied states. On the basis of these data, several absorption lines of the $v = 0 \rightarrow 1$ vibronic band of the $X^2\Sigma_g^+ \rightarrow B^2\Sigma_u^+$ transition were found to be coincident with the absorption peaks in the spectrum of the carbon star HD 56126.

In this study [51], the dipole moment function for C_2^- is close to 1 a.u. in the potential minimum area, thus the difference in intensities between FC approximation and the approach in which the transition moment is involved is negligible. On the other hand, the transition moment for the $A^3\Sigma^+ \leftrightarrow X^3\Pi$ transition in CO^{2+} as calculated by Cossart *et al.* [53] is approximately 0.26 Debye (i.e. 0.1 a.u.), hence the effect should be in one order of magnitude. Moreover, the line widths of dications are deeply affected by the finite lifetimes of excited states. The higher vibronic states can have their widths in the order of $10^{-2}\,cm^{-1}$, which is comparable with Doppler broadening at standard temperature. Therefore, during spectral analysis and attempts to identify the CO^{2+} dication, these short lifetimes of quasibound vibronic states should be taken into account.

Chapter 6

Theory

6.1 Coupled potential matrix

An effective Hamiltonian can be given as a sum of several parts

$$\hat{H}_{eff} = \hat{V}_{eff} + \hat{T} = \hat{H}_{el} + \hat{H}_{SO} + \hat{H}_{rot} + \hat{T}, \tag{6.1}$$

where $\hat{T}$ is kinetic operator, $\hat{H}_{el}$ is the purely electronic Hamiltonian, $\hat{H}_{SO}$ is the spin-orbit Hamiltonian, in the Hund's coupling case (a) defined as

$$\hat{H}_{SO} = H_{SOi} + A\hat{L}\hat{S}, \tag{6.2}$$

where H_{SOi} are interstates spin-orbit couplings and A is the spin-orbit spliting constant for the $X^3\Pi$ state in the CO^{2+} dication. The rotational Hamiltonian, $\hat{H}_{rot}$, is conveniently divided into two terms [54]

$$\hat{H}_{rot} = \hat{H}^0_{rot} + \hat{H}_{cor} = B(\hat{J} - \hat{L} - \hat{S})^2, \tag{6.3}$$

$$\hat{H}^0_{rot} = B(J^2 - J_z^2 + L^2 - L_z^2 + S^2 - S_z^2), \tag{6.4}$$

$$\hat{H}_{cor} = B[(L_+S_- + L_-S_+) - (J_+L_- + L_-J_+) - (J_+S_- + J_-S_+)], \tag{6.5}$$

where $J_\pm = J_x \pm iJ_y$, $L_\pm = L_x \pm iL_y$ and $S_\pm = S_x \pm iS_y$ are ladder operators with $\hat{J}$, $\hat{L}$ and $\hat{S}$ being total, electronic orbital and spin angular momenta, respectively. $\hat{H}_{cor}$ represents the heterogeneous perturbation (Coriolis interaction) between the two states [55] and $B = 1/(2\mu R^2)$ being rotation constant.

Most of the matrix elements of the rotational Hamiltonian (6.6) can be obtained based on general considerations of the matrix elements of an angular momentum operator in a basis set characterised by a quantum number specifying the total magnitude of the angular momentum ($\hat{J}$, $\hat{L}$ and $\hat{S}$) and a quantum number specifying the projection along the z axis (Ω, Λ and Σ, respectively) [55]. For example, the only non-vanishing matrix elements of the components of the spin angular momentum operator $\hat{S}$ in such a basis set are the following

$$\langle S\Sigma|S^2|S\Sigma\rangle = h^2S(S+1). \tag{6.6}$$

$$\langle S\Sigma|S_z|S\Sigma\rangle = \hbar\Sigma, \tag{6.7}$$

$$\langle S\Sigma \pm 1|S_\pm|S\Sigma\rangle = \hbar[(S \mp \Sigma)(S \pm \Sigma + 1)]^{1/2}. \tag{6.8}$$

The non-vanishing matrix elements of the components of the orbital angular momentum $\hat{L}$ can be obtained from (6.6–6.8) by replacing S by L, and Σ by Λ everywhere. The non-vanishing matrix elements of the total angular momentum $\hat{J}$ can be obtained from (6.9–6.11) by replacing S by J, and Σ by Ω everywhere, with the exception of $S_\pm$ having to be replaced by $J_\mp$ in the third equation

$$\langle J\Omega \pm 1|J_\mp|J\Omega\rangle = \hbar[(J \mp \Omega)(J \pm \Omega + 1)]^{1/2}. \tag{6.9}$$

This rather surprising difference in the behaviour of J as against L and S is discussed by Van Vleck [56].

In the case of the CO^{2+} dication, the six lowest electronic states split into 17 molecular states. These states divide into two non-interacting subgroups e, f due to parity with respect to the space inversion operator

e : $A^3\Sigma_1^+$, $c^1\Delta_2$, $b^1\Pi_1$, $a^1\Sigma_0^+$, $^3\Sigma_1^-$, $^3\Sigma_0^-$, $X^3\Pi_2$, $X^3\Pi_1$ and $X^3\Pi_0$

f : $A^3\Sigma_1^+$, $A^3\Sigma_0^+$, $c^1\Delta_2$, $b^1\Pi_1$, $^3\Sigma_1^-$, $X^3\Pi_2$, $X^3\Pi_1$ and $X^3\Pi_0$.

The subscript denotes $\Omega = |\Lambda + \Sigma|$. As $\Omega \leq J$ is required, some states do not exist for $J < 2$. Note that the states $a^1\Sigma_0^+$ and $^3\Sigma_0^-$ are presented only in the e parity block and also that $A^3\Sigma_0^+$ exists in the f parity block only. The matrix elements in a Hund's case (a) basis set obey the selection rule $\Delta\Sigma = 0$, or to put it differently $\Delta\Omega = \Delta\Lambda$ [57]. For example, the state $^1\Delta$ has only $\Omega = 2$. The lower triangle of the potential matrix V_{eff} in the symmetry-adapted basis is given in Table 6.1 for e parity and in Table 6.2 for f parity. The rovibronic energies and lifetimes have been calculated using e-s method described in chapter 2.

6.2 Probability of a transition

State-to-state transition probability $A(i \to f)$ is defined by the absolute value square of transition moment, such that

$$A(i \to f) = K\,\omega_{i\to f}^3\,|\langle v_i|\mu_{TM}(R)|v_f\rangle|^2, \tag{6.10}$$

where $\mu_{TM}(R)$ is the *ab initio* electronic transition moment calculated using `MOLPRO` suit [40]; ω is given by the transition frequency defined as $\hbar\omega = E_i - E_f$; and the multiplication constant $K = 7.2356 \times 10^{-6}$ is the appropriate factor to express the probability in s^{-1}, when the transition moment is given in units of eÅ, and the energy in cm^{-1}. In the case of the CO^{2+} dication, v_i and v_f represent continuum rovibronic states, as the diatomic is allowed to dissociate on all potential surfaces. Thus $A(i \to f) \equiv A(E_i \to E_f)$ defines the continuum-to-continuum emission probabilities for the transition between the rovibronic energies E_i and E_f.

In the case of narrow non-overlapping resonances, it is reasonable to assume that the system is preferentially prepared in close resonance energies, where the density

Table 6.1: Matrix elements of V_{eff} in the Hund's case (a) basis set for e parity. $U(^3\Sigma^+)$, $U(^1\Pi)$, etc. are BO potentials. H_{SO1-10} marks s-o interaction between particular states. A is spin-orbit constant of the $X^3\Pi$ state passed from Cossard *et al.* [53], $z = J(J+1)$ and $B = 1/2\mu R^2$.

	$\vert^3\Sigma_1^+\rangle$	$\vert^1\Delta_2\rangle$	$\vert^1\Pi_1\rangle$	$\vert^3\Sigma_1^-\rangle$	$\vert^3\Sigma_0^-\rangle$	$\vert^3\Pi_2\rangle$	$\vert^3\Pi_1\rangle$	$\vert^3\Pi_0\rangle$	$\vert^1\Sigma_0^+\rangle$
$\langle^3\Sigma_1^+\vert$	$U(^3\Sigma^+)+Bz$								
$\langle^1\Delta_2\vert$	0	$U(^1\Delta)+B(z+6)$							
$\langle^1\Pi_1\vert$	H_{SO1}	$-B2\sqrt{x-2}$	$U(^1\Pi)+Bz$						
$\langle^3\Sigma_1^-\vert$	H_{SO2}	0	H_{SO3}	$U(^3\Sigma^-)+Bz$					
$\langle^3\Sigma_0^-\vert$	$H_{SO2}-B\sqrt{2z}$	0	H_{SO3}	$-B\sqrt{2z}$	$U(^3\Sigma^-)+B(z+2)$				
$\langle^3\Pi_2\vert$	$H_{SO4}-B\sqrt{2(z-2)}$	H_{SO5}	H_{SO6}	$H_{SO6}-B\sqrt{2(z-2)}$	H_{SO7}	$U(^3\Pi)+A+B(z-2)$			
$\langle^3\Pi_1\vert$	$H_{SO4}+2B$	H_{SO5}	H_{SO6}	$H_{SO6}+2B$	$H_{SO7}-B\sqrt{2z}$	$-B\sqrt{2(z-2)}$	$U(^3\Pi)+B(z+2)$		
$\langle^3\Pi_0\vert$	$H_{SO4}+B\sqrt{2z}$	H_{SO5}	H_{SO6}	$H_{SO6}+B\sqrt{2z}$	$H_{SO7}+2B$	0	$-B\sqrt{2z}$	$U(^3\Pi)-A+B(z+4)$	
$\langle^1\Sigma_0^+\vert$	H_{SO8}	0	$-B\sqrt{2z}$	H_{SO9}	H_{SO9}	H_{SO10}	H_{SO10}	H_{SO10}	$U(^1\Sigma^+)+Bz$

Table 6.2: Matrix elements of V_{eff} in the Hund's case (a) basis set for f parity. $U(^3\Sigma^+)$, $U(^1\Pi)$, etc. are BO potentials. H_{SO1-7} marks s-o interaction between particular states. A is spin-orbit constant of the $X^3\Pi$ state passed from Cossard *et al.* [53], $z = J(J+1)$ and $B = 1/2\mu R^2$.

	$\vert^3\Sigma_1^+\rangle$	$\vert^1\Delta_2\rangle$	$\vert^1\Pi_1\rangle$	$\vert^3\Sigma_1^-\rangle$	$\vert^3\Pi_2\rangle$	$\vert^3\Pi_1\rangle$	$\vert^3\Pi_0\rangle$	$\vert^3\Sigma_0^+\rangle$
$\langle^3\Sigma_1^+\vert$	$U(^3\Sigma^+)+Bz$							
$\langle^1\Delta_2\vert$	0	$U(^1\Delta)+B(z+6)$						
$\langle^1\Pi_1\vert$	H_{SO1}	$-B2\sqrt{x-2}$	$U(^1\Pi)+Bz$					
$\langle^3\Sigma_1^-\vert$	H_{SO2}	0	H_{SO3}	$U(^3\Sigma^-)+Bz$				
$\langle^3\Pi_2\vert$	$H_{SO4}-B\sqrt{2(z-2)}$	H_{SO5}	H_{SO6}	$H_{SO7}-B\sqrt{2(z-2)}$	$U(^3\Pi)+A+B(z-2)$			
$\langle^3\Pi_1\vert$	$H_{SO4}+2B$	H_{SO5}	H_{SO6}	$H_{SO7}+2B$	$-B\sqrt{2(z-2)}$	$U(^3\Pi)+B(z+2)$		
$\langle^3\Pi_0\vert$	$H_{SO4}-B\sqrt{2z}$	H_{SO5}	H_{SO6}	$H_{SO7}-B\sqrt{2z}$	0	$-B\sqrt{2z}$	$U(^3\Pi)-A+B(z+4)$	
$\langle^3\Sigma_0^+\vert$	$-B\sqrt{2z}$	0	H_{SO1}	$H_{SO2}-B\sqrt{2z}$	H_{SO4}	$H_{SO4}-B\sqrt{2z}$	$H_{SO4}+2B$	$U(^3\Sigma^+)+B(z+2)$

of continuum states is very high. Similarly, we may assume that the spontaneous emission preferentially leads to predissociation states of the ground electronic surface in close proximity of resonances. Therefore, in the case of narrow resonances, it is sensible to define the integral resonance-to-resonance emission probability such that

$$A_{\text{int}}(r_i \to r_f) = \int_{\epsilon_{ri}-a\Gamma_{ri}}^{\epsilon_{ri}+a\Gamma_{ri}} dE_i \int_{\epsilon_{rf}-a\Gamma_{rf}}^{\epsilon_{rf}+a\Gamma_{rf}} dE_f \; A(E_i \to E_f), \tag{6.11}$$

where we integrate the continuum-to-continuum emission probabilities in the vicinity of the two participating resonances. ϵ_{ri} and ϵ_{rf} represent the positions of the two participating resonances, while Γ_{ri} and Γ_{rf} represent their widths. The factor $a \gg 1$ is adjusted such that only single resonances i and f contribute to $A_{\text{int}}(r_i \to r_f)$.

The integral emission probabilities $A_{\text{int}}(r_i \to r_f)$ are to be evaluated based on complex scaled non-hermitian resonance wavefunctions. To the best of our knowledge, continuum-to-continuum transition probabilities are not suitably defined using the complex scaled wavefunctions. However, the exact formula for continuum-to-bound state transition probabilities is available, derived e.g. by Andric et al. [58]:

$$A(i \to f) = K\,\omega_{i\to f}^3 \sum_{ri=1}^{N} \frac{\Im C_{ri,f}(E_i - \epsilon_{ri}) - \Re C_{ri,f}\Gamma_{ri}/2}{(E_i - \epsilon_{ri})^2 + \Gamma_{ri}^2/4}, \tag{6.12}$$

where the sum is over resonances and discretised states of rotated continuum on the excited electronic surface. $C_{ri,f}$ is given by,

$$C_{ri,f} = (\psi_{ri}^{(l)}|\mu_{TM}(Re^{i\theta})|\psi_f^{(r)})(\psi_f^{(l)}|\mu_{TM}(Re^{i\theta})|\psi_{ri}^{(r)}), \tag{6.13}$$

where ψ_{ri} and ψ_f represent the complex scaled resonance (initial) and bound (final) states given by solution of $\hat{H}_{eff\theta}$ defined by equation 2.1 with $\hat{V}_{eff}$ described using matrix in Tables 6.1 and 6.2. The indices (l) and (r) denote the left and right solutions of the non-hermitian complex scaled Hamiltonian, respectively, as defined in Ref. [30]. The left vector is defined as solution of the transposed complex scaled Hamiltonian. The wavefunctions are normalized such that $(\psi^{(l)}|\psi^{(r)}) = 1$. A special bracket notation has been used, where the 'bra' wavefunction is not complex conjugate as usual.

We are about to calculate emission probabilities to the lowest resonance on the ground state electronic surface which is extremely narrow, therefore we completely neglect its finite width and use Eq. 6.12 in substitution for the continuum-to-continuum Einstein coefficients in the definition of the integral emission probability, Eq. 6.11. Neglecting the energy dependence of the prefactor $\omega_{i\to f}^3$, we obtain:

$$A_{\text{int}}(r_i \to r_f) \approx K\,\omega_{ri\to rf}^3 (\psi_{ri}^{(l)}|\mu_{TM}(Re^{i\theta})|\psi_{rf}^{(r)})(\psi_{rf}^{(l)}|\mu_{TM}(Re^{i\theta})|\psi_{ri}^{(r)}), \tag{6.14}$$

where ψ_{rf} is the final resonance wavefunction with position given by ϵ_{rf} and $\hbar\omega_{ri\to rf} = \epsilon_{ri} - \epsilon_{rf}$.

The integral Einstein coefficients enable calculation of the radiative lifetimes associated with individual resonances on excited electronic states, such that $\tau_{ri} = 1/A_{\text{int}}(r_i \to r_f)$ [59].

6.3 Intensities

The intensities of the studied rovibronic absorption transitions have been calculated using the well-known formula [57]

$$I_{abs}^{i\to f} = I_0 \frac{8}{3}\frac{\pi^3}{hc} S_J N_{J''v''} S_J \omega_{ri\to rf}^3 t_{ri,f}^2, \tag{6.15}$$

where I_0 is the intensity of the source, $t_{ri,f}$ is the appropriate transition matrix element defined according to previous deduction Eq. 6.14, $N_{J''v''}$ is the number of molecules in the initial rovibronic state $|v_{ri}\rangle$ determined using the Boltzmann distribution law

$$N_{J''v''} = \frac{N}{q^r q^v}(2J+1)e^{-E_{J''v''E''}/kT}, \tag{6.16}$$

with N as the total number of molecules CO^{2+} in the sample, q^r and q^v being rotational and vibrational partition functions, k and T being Boltzmann constants and temperature, respectively. S_J are Hönl-London factors ($S_J = (2J+1)/4$ for the Q branch in electronic transitions, where $\Delta\Lambda = \pm 1$). Within the studied electronic states of CO^{2+}, the partition functions can be written as

$$q^r \approx \frac{kT}{hcB}, \tag{6.17}$$

$$q^v \approx \frac{1}{1-e^{\frac{hc\nu}{kT}}}. \tag{6.18}$$

Chapter 7

Calculated spectra

We have been interested in $A^3\Sigma^+ \rightarrow X^3\Pi$ (A–X) and $b^1\Pi \rightarrow a^1\Sigma^+$ (b–a) rovibronic transitions in the CO^{2+} dication which are spin-allowed and belong to Vis and IR spectra, respectively. However, according to the results in Ref. [60] (enclosed as Paper 3), spin-forbidden transitions could also be detected. The transition moment elements of these transitions are lower by only about 3 orders of magnitude and therefore their peaks could be found in high-resoluted spectra. In that work, the transition matrix elements were determined using several different approaches ("exact", Franck-Condon (FC) and two-state approximation). The results were that the FC approximation was found inadequate in the case of spin-allowed transitions. On the other hand, in the case of two state approximation, which include two electronic states participating in the transition, the resulting values were fairly reasonable. The following calculations have been carried out using the "exact" transition matrix elements calculated as a six-dimensional approach.

7.1 Emission spectra

Unfortunately, it seems that emission spectra from the examined electronic states ($A^3\Sigma^+$ and $b^1\Pi$) cannot be created, as can be extrapolated from our previous study [60] that is oriented mainly on calculations of radiative lifetimes from these states. These lifetimes are longer than the predissociation ones. Hence, in other words, a dication decays before it can emit a photon. Neither after the involvement of the rotation effect are the rovibronic states stable enough. Only one rovibronic state $A^3\Sigma^+$, $v = 0$ $J = 1$ has predissociated lifetime in order of μs and this value is comparable with radiative lifetime.

Nevertheless, there is still an opportunity to measure emission peaks pertaining to $d^1\Sigma^+ \rightarrow a^1\Sigma^+$, $e^1\Sigma^+ \rightarrow a^1\Sigma^+$ and/or $e^1\Sigma^+ \rightarrow d^1\Sigma^+$. These translations should occur around 32341 cm^{-1} (309 nm), 48855 cm^{-1} (204 nm) and 16513 cm^{-1} (605 nm), respectively. As far as theoretical prediction is concerned, in the case of the $d^1\Sigma^+$ state, there will be difficulties with double minimum potential energy curves, whereas $e^1\Sigma^+$ state is so highly excited that general problems with calculating will appear.

These calculations will probably be performable in the near future.

7.2 Absorption spectra

An exampel of the successfully calculated absorption spectra in the visible and infrared part of electromagnetic radiation are shown in Figs. 7.1 to 7.6. As for other transitions, the frequencies are possible to derivate from the spectroscopic constants collected in Table I Ref. [34]. The intensities are calculated as absolute due to the equation (6.10). The independent variables are the volume of the sample (the number of particles) and temperature. The $I_0 = 1$, $T = 300\,\mathrm{K}$ and $N = 10^{10}$ particles of CO^{2+} have been used for all the calculations in this study. Since after excitation into higher electronic states, the systems become unstable and dissociate before they can emit a photon, the absorption spectra can be regarded as photodissociation spectra.

The vibronic spectra of the A←X and b←a transitions are shown in Figs. 7.1 and 7.4, respectively. The intensities are depicted as their natural logarithms, so that the differences between them can be clearly recognised. The corresponding energy positions, widths and intensities are summarised in Table 7.1. A part of Fig. 7.1 for $v = 0$, i.e. the rovibronic spectrum, is shown in more detail in Fig. 7.2. The peaks for $J = 1$ and 2 are not in the following figure 7.3, where the profiles are demonstrated. In the case of A←X transition, the highest intensity is for $J = 1$ rovibronic states, and then the intensities exponentially decrease, which is caused by the fact that the width of $J = 1$ is narrower than that of the others. This effect of predissociation in the rotational states within the A electronic state provides a counterbalance to the classical example of intensity distribution due to temperature.

One of these examples is shown in Fig. 7.5, where the intensities increase with J increasing up to $J_{\max}$. In this case of the b←a transition, $J_{\max}$ is around 10 (for $T = 300\,\mathrm{K}$). This figure is not a detail of the previous one, 7.4, because the rotational states within $v = 0$ have very narrow widths, at the limits of the precision of the methods used. On the other hand, the $v = 1$ 1 could be used, however, although the state $a^1\Sigma^+$, $v = 1$ has a long lifetime, it is better to use an even longer one if it exists. The shapes of rotational states are drawn in Fig. 7.6. Each J-line shape is in the same colour in the figures 7.3 and 7.6 for the sake of comparison between the transitions. The corresponding energy positions, widths and intensities are summarised in Table 7.2.

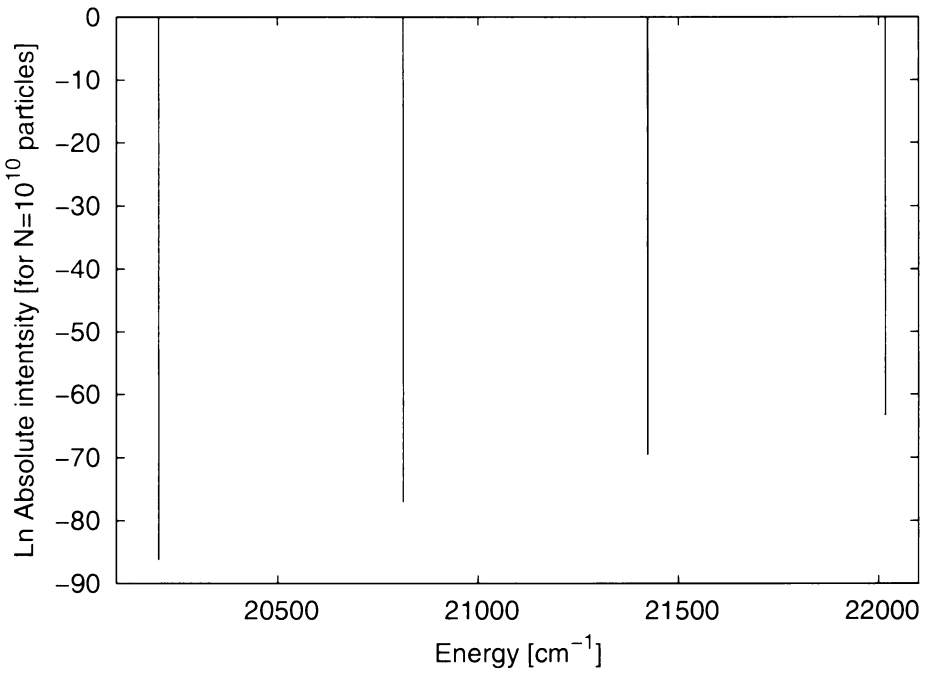

Figure 7.1: The vibronic absorption spectra of $A^3\Sigma^+ \leftarrow X^3\Pi$ transition in CO^{2+}. The absolute intensities are depicted as natural logarithms, so that the differences between them can be clearly seen.

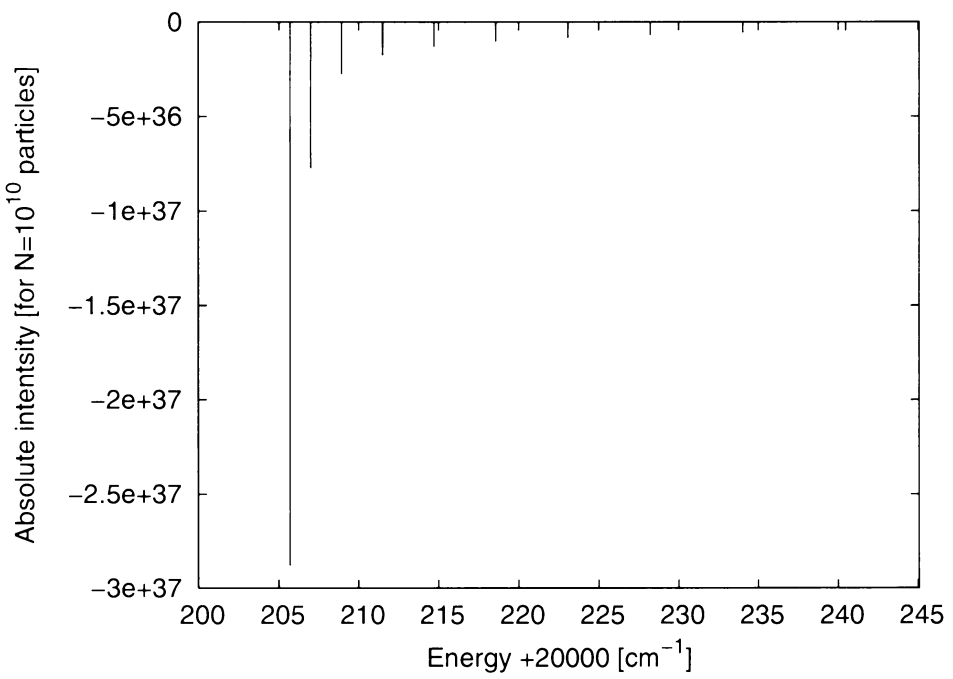

Figure 7.2: The rovibronic absorption spectrum of $A^3\Sigma^+$, $v = 0 \leftarrow X^3\Pi$, $v = 0$.

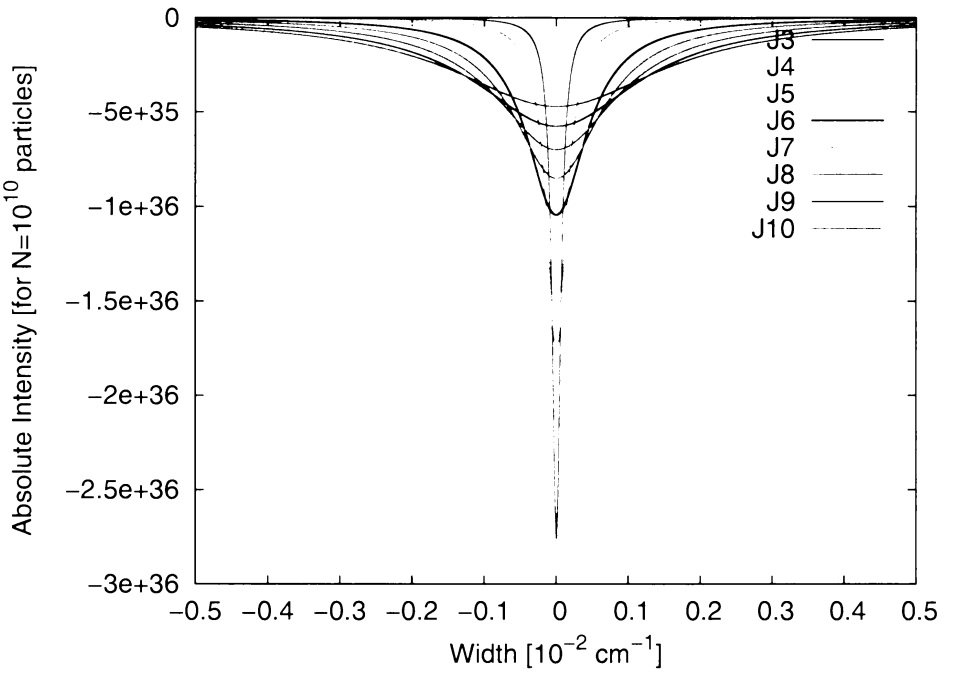

Figure 7.3: The widths of the rovibronic spectra shown in Fig. 7.2.

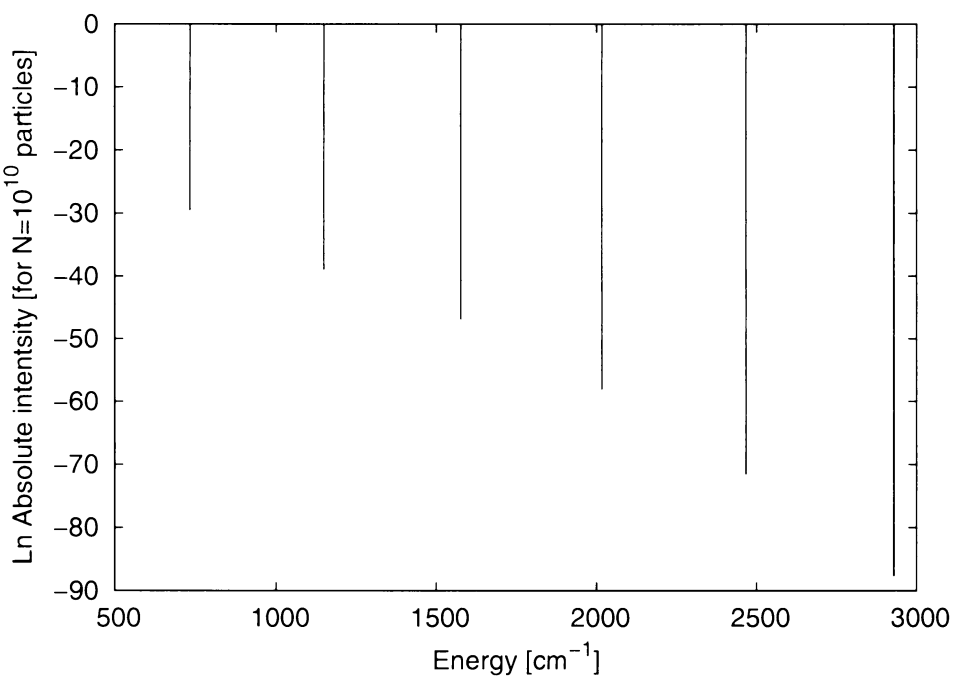

Figure 7.4: The vibronic absorption spectra of $b^1\Pi \leftarrow a^1\Sigma^+$ transition in CO^{2+}. The absolute intensities are depicted as natural logarithms, so that the differences between them can be clearly seen.

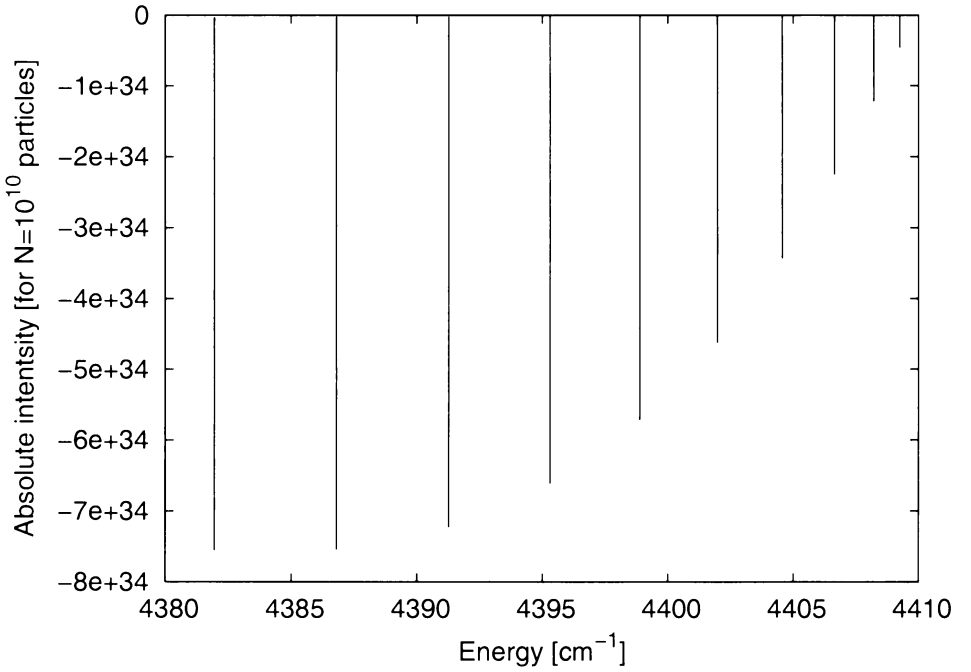

Figure 7.5: The rovibronic absorption spectrum of $b^1\Pi$, $v = 1 \leftarrow a^1\Sigma^+$, $v = 0$.

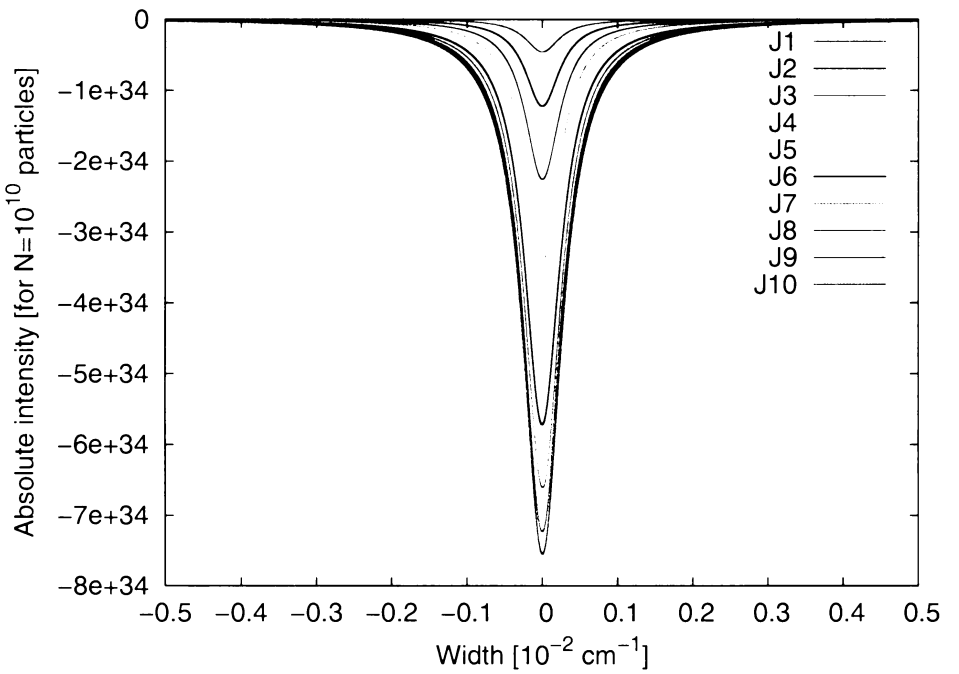

Figure 7.6: The widths of the rovibronic spectra displayed in Fig. 7.5.

Table 7.1: The energies (cm^{-1}), widths (cm^{-1}) and absorption absolute intensities of the vibronic transitions A←X and b←a for $I_0 = 1$, $T = 300\,K$ and $N = 10^{10}$ particles of CO^{2+} calculated by Eq. 6.15. Values are ilustrated in Fig. 7.1 and 7.4.

	A←X			b←a		
v	E(cm^{-1})	Γ(cm^{-1})	Intensity	E(cm^{-1})	Γ(cm^{-1})	Intensity
0	20205.04	7.5×10^{-5}	-7.05×10^{33}	2929.13	1.7×10^{-7}	-1.34×10^{32}
1	20813.07	7.9×10^{-4}	-7.39×10^{30}	2466.58	1.3×10^{-4}	-1.01×10^{28}
2	21423.00	1.9×10^{-3}	-1.02×10^{28}	2016.65	8.2×10^{-3}	-9.23×10^{23}
3	22017.48	1.7×10^{-3}	-1.73×10^{25}	1576.69	6.4×10^{-2}	-9.90×10^{19}
4				1148.57	2.4×10^{-2}	-1.23×10^{16}
5				733.21	3.8×10^{-2}	-1.66×10^{12}

Table 7.2: The energies (cm^{-1}), widths (cm^{-1}) and absorption absolute intensities of the rovibronic transitions A←X $\Delta v = 0$ and b←a $\Delta v = 1$, $\Delta\Omega = 0$ Q branch for $I_0 = 1$, $T = 300\,K$ and $N = 10^{10}$ particles of CO^{2+} calculated by Eq. 6.15. Values are ilustrated in Fig. 7.2, 7.3, 7.5 and 7.6.

	A←X			b←a		
J	E(cm^{-1})	Γ(cm^{-1})	Intensity	E(cm^{-1})	Γ(cm^{-1})	Intensity
1	20205.69	0.13×10^{-5}	-1.19×10^{32}	4409.25	2.72×10^{-4}	-3.94×10^{30}
2	20206.98	1.32×10^{-5}	-3.22×10^{32}	4408.21	2.75×10^{-4}	-1.05×10^{31}
3	20208.92	6.97×10^{-5}	-6.04×10^{32}	4406.64	2.77×10^{-4}	-1.96×10^{31}
4	20211.49	1.70×10^{-4}	-9.40×10^{32}	4404.56	2.81×10^{-4}	-3.02×10^{31}
5	20214.71	3.15×10^{-4}	-1.30×10^{33}	4401.97	2.85×10^{-4}	-4.14×10^{31}
6	20218.58	5.05×10^{-4}	-1.65×10^{33}	4398.88	2.90×10^{-4}	-5.21×10^{31}
7	20223.08	7.42×10^{-4}	-1.98×10^{33}	4395.30	2.95×10^{-4}	-6.14×10^{31}
8	20228.23	10.2×10^{-4}	-2.26×10^{33}	4391.26	3.01×10^{-4}	-6.85×10^{31}
9	20234.02	13.6×10^{-4}	-2.46×10^{33}	4386.79	3.08×10^{-4}	-7.32×10^{31}
10	20240.46	17.4×10^{-4}	-2.58×10^{33}	4381.94	3.16×10^{-4}	-7.52×10^{31}

List of Abbreviations

1D	one dimensional
c-s	complex-scaling
CAS SCF	Complete Active Space Self-Consistent Field
cc-pV(5 or 6)Z	correlation-consistent polarized valence (quintuple or sextuple)-split basis s
FC	Franck-Condon approximation
icMRCI	internally contracted Multi-Reference Configuration Interaction
IR	Infrared
ISM	Interstelar medium
PAH	Polycyclic Aromatic Hydrocarbon
PEF	Potential energy function
s-o	spin-orbit interaction
UVIS	Ultraviolet and visible
WKB	Wentzel Kramers Brillouin (approximation)

References

[1] Vaughan, A. L. *Phys. Rev.* **38**, 1687 (1931).

[2] Mathur, D. *Phys. Rep.* **391**, 1 (2004).

[3] Mathur, D. *Phys. Rep.* **225**, 193 (1993).

[4] Avakyan, S. V. *J Opt. Tech.* **65**, 870 (1998).

[5] Lilensten, J., Witasse, O., Simon, C., Soldi-Lose, H., Dutuit, O., Thissen, R., and Alcaraz, C. *Geophys. Research Lett.* **32**, L03203 (2005).

[6] Witasse, O., Dutuit, O., Thissen, R., Žabka, J., Alcaraz, C., and Lilensten, J. *EGS XXVII General Assembly* **abstract No. 3115** (2002).

[7] Petrie, S. and Bohme, D. K. *Astrop. J.* **540**, 869 (2000).

[8] Malloci, G., Joblin, C., and Mulas, G. *Astro. Astrophys.* (2006).

[9] Bakes, E. L. O. and Tielens, A. G. G. M. *Ap. J.* **427**, 822 (1994).

[10] Price, S. D. *Phys. Chem. Chem. Phys.* **5**, 1717 (2003).

[11] Šedivcová, T., Žďánská, P. R., Špirko, V., and Fišer, J. *J. Chem. Phys.* **124**, 214303 (2006).

[12] Bell, C., Cory, M., Fairley, T., Hall, J., and Tidwell, R. *Antimicrob. Agents Chemother.* **35**, 1099 (1991).

[13] Brendle, J. J., Outlaw, A., Kumar, A., Boykin, D. W., Patrick, D. A., Tidwell, R. R., and Werbovetz, K. A. *Antimicrob. Agents Chemother.* **46**, 797 (2002).

[14] Boykin, D., Kumar, A., Xiao, G. W. D., Bender, B., McCurdy, D., Hall, J., and Tidwell, R. *J. Med. Chem.* **41**, 124 (1998).

[15] Blagburn, B. L., Drain, K. L., Land, T. M., Kinard, R. G., Moore, P. H., Lindsay, D. S., Boykin, D. W., and Tidwell, R. R. *Antimicrob. Agents Chemother.* **42**, 2877 (1998).

[16] Bell, C. A., Hall, J. E., Kyle, D., Grogl, M., Ohemeng, K., Allen, M., and Tidwell, R. *Antimicrob. Agents Chemother.* **34**, 1381 (1990).

[17] Price, S. D. *J. Chem. Soc., Faraday Trans.* **93**, 2451 (1997).

[18] Schröder, D. and Schwarz, H. *J. Phys. Chem. A* **103**, 7385 (1999).

[19] Nicolaides, C. A. *Chem. Phys. Lett.* **161**, 547 (1989).

[20] Wong, M. W. and Radom, L. *J. Chem. Phys.* **93**, 6303 (1989).

[21] Helm, H., Stephan, K., Märk, T. D., and Huestis, D. L. *J. Chem. Phys.* **74**, 3844 (1981).

[22] Hagan, D. A. and Eland, J. H. D. *Rapid Commun. Mass Spect.* **3**, 186 (1989).

[23] Hishikawa, A., Hasegawa, H., and Yamanouchi, K. *Chem. Phys. Letters* **361**, 245 (2002).

[24] Andersen, L. H., Posthumus, J. H., Vahtras, O., Ågren, H., Elander, N., Nunez, A., Scrinzi, A., Natiello, M., and Larsson, M. *Phys. Rev. Lett.* **71**, 1812 (1993).

[25] Bouhnik, J. P., Gertner, I., Rosner, B., Amitay, Z., Heber, O., Zajfman, D., Sidky, E. Y., and Ben-Itzhak, I. *Phys. Rev. A* **63**, 032509 (2001).

[26] Child, M. S. *Semiclassical Mechanics with Molecular Applications, Clarendon Press, Oxford* (1991).

[27] Hazi, A. U. and Taylor, H. S. *Phys. Rev. A* **1**, 1190 (1970).

[28] Lefebvre, R. *J. Phys. Chem.* **89**, 4201 (1985).

[29] Mandelshtam, A., Taylor, H. S., Ryaboy, V., and Moiseyev, N. *Phys. Rev. A* **50**, 2764 (1994).

[30] Moiseyev, N. *Phys. Rep.* **302**, 211 (1998).

[31] Ryaboy, V. and Moiseyev, N. *J. Chem. Phys.* **103**, 4061 (1995).

[32] Dalitz, R. H. and Moorhouse, R. G. *Proc. R. Soc. A* **318**, 279 (1970).

[33] Šedivcová, T., Špirko, V., and Fišer, J. *J. Chem. Phys.* **125**, 164308 (2006).

[34] See EPAPS Document No. E-JCPSA6-124-008618 for the results comprising a complete set of the spectroscopic constants of the probed electronic states and details illustrating the stabilisation and complex-scaling procedures used in the present study. This document can be reached via a direct link in the online article's HTML reference section or via the EPAPS homepage (http://www.aip.org/pubservs/epaps.html).

[35] Barinovs, Ğ. and Hemert, M. C. *Chem. Phys. Lett.* **399**, 406 (2004).

[36] Li, Y., Bludský, O., Hirsch, G., and Buenker, R. J. *J. Chem. Phys.* **107**, 3014 (1997).

[37] Baccarelli, I., Andric, L., Grozdanov, T. P., and McCarroll, R. *J. Chem. Phys.* **117**, 3013 (2002).

[38] Bludský, O., Li, Y., Hirsch, G., and Buenker, R. J. *J. Chem. Phys.* **109**, 1201 (1998).

[39] Moiseyev, N. *J. Phys. B: At. Mol. Opt. Phys.* **31**, 1431 (1997).

[40] Werner, H.-J., Knowles, P. J., Lindh, R., Schütz, M., Celani, P., Korona, T., Manby, F. R., Rauhut, G., Amos, R. D., Bernhardsson, A., Berning, A., Cooper, D. L., Deegan, M. J. O., Dobbyn, A. J., Eckert, F., Hampel, C., Hetzer, G., Lloyd, A. W., McNicholas, S. J., Meyer, W., Mura, M. E., Nicklass, A., Palmieri, P., Pitzer, R., Schumann, U., Stoll, H., Stone, A. J., Tarroni, R., and Thorsteinsson, T. Molpro, version 2002.6, a package of ab initio programs, (2003), see http://www.molpro.net.

[41] Dunning, Jr., T. H. *J. Chem. Phys.* **90**, 1007 (1989).

[42] Werner, H.-J. and Knowles, P. J. *J. Chem. Phys.* **89**, 5803 (1988).

[43] Knowles, P. J. and Werner, H.-J. *Chem. Phys. Lett.* **145**, 514 (1988).

[44] Johnson, B. R. *J. Chem. Phys.* **69**, 4678 (1978).

[45] Krishnamurthi, V., Krishnamurthy, M., Marathe, V., and Mathur, D. *J. Phys. B* **25**, 5149 (1992).

[46] Carroll, P. *Can. J. Phys.* **36**, 1585 (1958).

[47] Cossart, D., Bonneau, M., and Robbe, J. M. *J. Mol. Spec.* **125**, 413 (1987).

[48] Dujardin, G., Hellner, L., Hamdan, M., Brenton, A. G., Olsson, B. J., and Besnard-Ramage, M. J. *J. Phys. B* **23**, 1165 (1990).

[49] Herman, Z., Jonathan, P., Brenton, A. G., and Beynon, J. H. *Chem. Phys. Lett.* **141**, 433 (1987).

[50] Cossart, D. and Cossart-Magos, C. *J. Mol. Spec.* **147**, 471 (1991).

[51] Šedivcová, T. and Špirko, V. *Mol. Phys.* **104**, 1999 (2006).

[52] Civiš, S., Hosaki, Y., Kagi, E., Izumiura, H., Yanagisawa, K., Šedivcova, T., and Kawaguchi, K. *Publ. Astron. Soc. Japan* **57**, 605 (2005).

[53] Cossart, D. and Robbe, J. M. *Chem. Phys. Lett.* **311**, 248 (1999).

[54] Carrington, A. and Softley, T. P. *Chem. Phys.* **106**, 315 (1986).

[55] Hougen, J. T. *The Calculation of Rotational Energy Levels and Rotational Line Intensities in Diatomic Molecules, US Natl. Bur. Stand. Monogr.* **115** (1979).

[56] Vleck, J. H. V. *Revs. Mod. Phys.* **23**, 213 (1951).

[57] Herzberg, G. Molecular spectra and molecular structure volume i - spectra of diatomic molecules, (Robert E. Krieger Publishing company, 1989).

[58] Andric, L., Baccarelli, I., Grozdanov, T. P., and McCarroll. *Phys. Lett. A* **298**, 41 (2002).

[59] Zemke, W. T. and Stwalley, W. C. *J. Chem. Phys.* **120**, 88 (2004).

[60] Šedivcová, T., Špirko, V., and Žďánská Kaprálová, P. R. *J. Mol. Spec.* **submited** (2006).

[61] Reinhard, W. P. *Ann. Rev. Phys. Chem.* **33**, 223 (1982).

[62] Peach, G. *Advances in Physics* **30**, 367 (1981).

Appendix A

Complex-scaling method

A.1 The basic idea

The simplest mathematical description of metastable states is that they resemble bound stationary states in that they are "localised" in space (at $t = 0$) and their time evolution is given by [61]

$$\upsilon_R(t) = \exp(-iE_R t/h)\upsilon_R(0), \tag{A.1.1}$$

which is the usual stationary state time dependence, except for the energy E_R of the resonant state now being complex

$$E_R = E_{res} - i\Gamma/2, \tag{A.1.2}$$

where E_{res} and Γ are real, and $\Gamma \geq 0$. The presence of the "$-i\Gamma/2$" forces exponential decay. If we assume that such a simple description of the time evolution is adequate, a prior calculation of the real and imaginary parts of E_R allows prediction of the formation energies and lifetimes of intermediate species. The complex coordinates in the non-relativistic quantum theory produce non-Hermitian operators, which have the energies of Eq. 2 among their actual eigenvalues.

The complex implementation of the real operators is carried out using Cauchy's theorem. If the operator is analytic in the independent variable (e.g., $V(R)$ in atomic distances R), the Hamiltonian can be rewritten in terms of contour integrals without changing the expected value of the energy.

A.2 Several approaches to avoid fitting *ab initio* potential

A.2.1 Scaling of basis functions

This approach comes from the substitution

$$V_{ij} = \int_{-\infty}^{\infty} \phi_i(x)V(xe^{i\theta})\phi_j(x)\,dx = e^{-i\theta}\int_{-\infty}^{\infty} \phi_i(xe^{i\theta})V(x)\phi_j(xe^{i\theta})\,dx. \tag{A.2.3}$$

The integration in the right-hand side term can be carried out on a grid

$$V_{ij} = e^{-i\theta} \sum_{\gamma=1}^{N_\alpha} w_\gamma \phi_i(x_\gamma e^{-i\theta}) V(x_\gamma) \phi_j(x_\gamma e^{-i\theta}), \tag{A.2.4}$$

where x_γ and w_γ are the points and weights, respectively. Despite the fact that only square-integrable basis functions can be used directly in complex dilatation [38], several authors use, e.g., the particle-in-box basis functions [31]. A good solution is reported by Li *et al.* [36]. They take a basis of complex-scaled harmonic oscillator functions

$$\phi_i(x) = e^{-\beta R^2/2} H_i(\beta^{1/2} x), \tag{A.2.5}$$

where $\beta = \sqrt{k\nu}$ with k and ν are the force constant and reduce mass of the Harmonic oscillator, respectively, and H_i is a Hermite polynom.

The numerical evaluation of the complex potential energy matrix elements using the gauss-Hermite quadrature is relatively straightforward. However, because of rounding errors in floating point arithmetic, numerical instabilities are encountered in the evaluation of the complex-scaled Hermite polynoms $H_i(\beta^{1/2} x e^{-i\theta})$, even for a basis set of a moderate size (typically for $J = 50$ in double-precision codes). Note that in our study we had to use 300 basis functions for a 5-dimensional problem.

A.2.2 Complex absorbing potential (CAP)

It is based on the introduction of the new complex absorbing potential $W(R)$ to the Hamiltonian (e.g. as defined by Eq. 2.1 in chapter 2), and using the newly modified $\hat{H}$

$$\hat{H}(x) = -\frac{1}{2\mu}\frac{d^2}{dx^2} + V(x) - iW(x), \tag{A.2.6}$$

where $W(x) > 0$ is a slowly increasing potential departing from zero only in the asymptotic region. For instance in Ref. [37], there was used an absorbing potential of a power form for a single-channel problem

$$W(x) = \begin{cases} 0, & R \pm R_a \\ \beta(R - R_a)^n, & R > R_a \end{cases}, \tag{A.2.7}$$

with β being a strength parameter and $n = 2$ or 4.

Its use is limited to one-dimensional problems or to a multichannel problem with a single dominant decaying channel. If this is not the case, we should take into consideration the fact that for each of the decaying channels, we need to define another $W(R)$.

A.2.3 Smooth-exterior-complex-scaling (SECS)

It consists in replacing the radial coordinate with the complex path

$$R \rightarrow F(R) \tag{A.2.8}$$

having the property $F(R) \to R\exp(i\theta)$ as $R \to \infty$ and where θ is a real rotation angle. If the derivative (Jacobian) is introduced

$$f(R) = \frac{dF}{dR} = 1 + [\exp(i\theta) - 1]g(R), \tag{A.2.9}$$

then the standard complex scaling method is obtained for $g(R) = 1$, whereas the selection of a $g(R)$ as a function varying from 0 to 1 in the narrow region around $R = R_0$, provides a SECS path.

The transformed Hamiltonian is given as

$$\hat{H} = -\frac{1}{4m}\left(\frac{1}{f^2}\frac{d^2}{dR^2} + \frac{d^2}{dR^2}\frac{1}{f^2}\right) + V_f(R) + V(F(R)), \tag{A.2.10}$$

with

$$V_f(R) = \frac{1}{4m}\left(\frac{7}{2}\frac{(f')^2}{f^4} - \frac{f''}{f^3}\right). \tag{A.2.11}$$

R_0 can be chosen large, so that $V(F(R)) \sim V(R)$, or it could be chosen in an asymptotic region, where the potential $V(R)$ is known analytically. The additional, mass-dependent complex potential $V_f(R)$ is strongly localised in the vicinity of $R = R_0$.

Appendix B

Intensity line profile

A line extends over a range of frequencies, not a single frequency. In addition, its centre may be shifted from its nominal central wavelength. There are several reasons for this broadening and shift:

Natural broadening: the easiest explanation is provided already by the classical electron theory, describing a radiating system as a classical harmonic oscillator, consisting of an electron and binding a quasielastic force to a stationary point. Concerning quantum mechanics, the uncertainty principle relates the life of an excited state with the precision of the energy. The widths depend on Einstein coefficients and radiative properties of a particular state in a particular system. This broadening effect is described by a Lorentzian profile, and there is no associated shift.

Thermal Doppler broadening: the atoms in a gas emitting radiation will have a distribution of velocities. Each photon emitted will be red or blue shifted by the Doppler effect, depending on the velocity of the atom relative to the observer. The higher the temperature of the gas, the wider the distribution of velocities in the gas. Since the spectral line is a combination of all the emitted radiation, the higher the temperature of the gas, the broader the spectral line emitted from that gas will be. This broadening effect is described by a Doppler profile, and there is no associated shift.

Pressure broadening: the presence of nearby particles will affect the radiation emitted by an individual particle. There are two limiting cases in which this occurs:

- *Impact pressure broadening:* the collision of other particles with the emitting particle interrupts the emission process. The duration of the collision is much shorter than the lifetime of the emission process. This effect depends on both the density and the temperature of the gas. The broadening effect is described by a Lorentzian profile and there may be an associated shift.

- *Quasistatic pressure broadening:* the presence of other particles shifts the energy levels in the emitting particle, thereby altering the frequency of the emitted radiation. The duration of the influence is much longer than the lifetime of the emission process. This effect depends on the density of the gas, but is

rather insensitive to temperature. The form of the line profile is determined by the functional form of the perturbing force with respect to the distance from the perturbing particle. There may also be a shift in the line centre. The Lévy skew alpha-stable distribution has been found to be a useful generalisation describing a quasistatic line profile [62].

Pressure broadening may also be classified by the nature of the perturbing force.

- *Linear Stark broadening* occurs via the linear Stark effect, resulting from the interaction of an emitter with an electric field, which causes a shift in energy that is linear in the field strength.
- *Quadratic Stark broadening* occurs via the quadratic Stark effect, resulting from the interaction of an emitter with an electric field, which causes a shift in energy that is quadratic in the field strength.
- *Van der Waals broadening* occurs when the emitting particle is being perturbed by Van der Waals forces. For the quasistatic case, a Van der Waals profile is often useful in describing the profile. The energy shift as a function of distance is given in the wings by e.g. the Lennard-Jones potential.

Opacity broadening: considerable reabsorption of emission line photons, an effect known as opacity, often causes line broadening. The line is broadened as photons at the line wings have a smaller reabsorption probability than photons at the line centre. Indeed, the absorption near the line centre may be so great as to cause a self-reversal, in which the intensity at the centre of the line is lesser than in the wings. This type of broadening is different from the above-mentioned broadening mechanisms, because it depends on the conditions along the entire path taken by the radiation, rather than simply on conditions that are local to the emitting particle.

These mechanisms can act in isolation or in combination. Assuming that each effect is independent of the other, the combined line profile will be the convolution of the line profiles of each mechanism. For example, a combination of thermal Doppler broadening and impact pressure broadening will yield a Voigt profile.

List of Publication

[1] Civiš S., Hosaki Y., Kagi E., Izumiura H., Yanagisawa K., Šedivcová T., Kawaguchi K.: Search for C_2^- in diffuse clouds. Publications of the Astronomical Society of Japan **57** (4): 605–609 (2005).

[2] Šedivcová T., Špirko V.: Potential energy and transition dipole moment functions of C_2^-, Molecular Physics **104** (13–14): 1999–2005 (2006).

[3] Šedivcová T., Žďánská P. R., Špirko V., Fišer J.: Computed lifetimes of metastable states of CO^{2+}, Journal of Chemical Physics **124** (21): Art. No. 214303 (2006).

[4] Šedivcová T., Špirko V., Fišer J.: Theoretical study of the CS^{2+} dication. Journal of Chemical Physics **125** (16): Art. No. 164308 (2006).

[5] Tada H., Kawaguchi K., Izumiura H., Civiš S., Šedivcová T.: Observational studies relating to diffuse interstellar bands. Astrochemistry. From laboratory studies to Astronomical Observations, AIP Conference Proceedings **855**: 219–224 (2006).

[6] Babanková D., Civiš S., Juha L., Bittner M., Cihelka J., Pfeifer M., Skála J., Bartnik A., Fiedorowicz H., Mikolajczyk J., Ryc L., Šedivcová T.: Optical and X-ray emission spectroscopy of high-power laser-induced dielectric breakdown in molecular gases and their mixtures. Journal of Physical Chemistry A **110**: 12113 (2006).

[7] Šedivcová T., Špirko V., Žďánská Kaprálová P. R.: Radiative properties of the CO^{2+} dication. Journal of molecular spectroscopy: submited.